JOURNAL OF APPLIED ELECTROCHEMISTRY **29**: 191–200, 1999.

Kinetics and mechanism of MnO_2 dissolution in H_2SO_4 in the presence of pyrite

B. B. NAYAK, K. G. MISHRA, R. K. PARAMGURU

Regional Research Laboratory, (Council of Scientific and Industrial Research), Bhubaneswar, 751 013, India

Received 10 April 1997; accepted in revised form 17 March 1998

This paper describes a study of the kinetics and mechanism of MnO_2 dissolution in H_2SO_4 in the presence of pyrite through leaching and electrochemical parameters. Manganese(IV) was found to dissolve mainly through reduction by the ferrous ion generated during oxidation of pyrite by the ferric ion. The oxidation which is slower and rate controlling may proceed through two different reactions, one producing S^0 and the other SO_4^{2-}. Manganese dissolution runs at the same rate as that of pyrite oxidation by maintaining ferrous ion concentration at a much lower level than that of ferric. Kinetic equations based on corrosion coupling principles are developed to explain the observed leaching behaviour.

Keywords: *cyclic redox reaction*, *dissolution*, *kinetics*, *manganese dioxide*, *mechanism*, *pyrite*

List of symbols

A electrode area
E electrode potential
F Faraday number
i current
k rate constant
K_1 constant, $Z_c A_c F k_{cf} (14 A_a k_{af})^{1/2}$
K_2 constant, $A_c k_{cf}$
K_3 constant, $14 A_a k_{ab}$
K_4 constant, $F A'_a (2 A'_c k_{cf})^{1/2}$
K_5 constant, $A'_a k'_{af}$
K_6 constant, $2 A'_c k'_{cb}$
K_7 constant, K_3/K_1^2
K_8 constant, K_2/K_1^2
K_9 constant, K_6/K_4^2
K_{10} constant, K_5/K_4^2
K_{11} constant
n number of electrons involved in the rate controlling step
R the universal gas constant
T absolute temperature
Z number of electrons involved in the reaction
β transfer coefficient

Subscripts/superscripts
a anodic
b backward reaction
c cathodic

corr corrosion
f forward reaction
g galvanic
′ refers to MnO_2 electrode

1. Introduction

The reduction leaching of MnO_2 from low grade ores in the presence of pyrite in acid medium is well-established [1–4]. Over 98% manganese may be leached successfully from low grade pyrolusite at a temperature of 100 °C within one hour [4]. The following reactions take place:

$$MnO_2 + 2\,Fe^{2+} + 4\,H^+ = Mn^{2+} + 2\,Fe^{3+} + 2\,H_2O \quad (1)$$

$$FeS_2 + 14\,Fe^{3+} + 8\,H_2O = 15\,Fe^{2+} + 16\,H^+ + 2\,SO_4^{2-} \quad (2)$$

$$FeS_2 + 2\,Fe^{3+} = 3\,Fe^{2+} + 2\,S^0 \quad (3)$$

Manganese dissolution occurs mainly through reduction by the ferrous ion (Reaction 1) generated during pyrite oxidation by the ferric ion (Reactions 2 and 3). As Reaction 1 is relatively faster, the slower FeS_2 oxidation reactions control the process and MnO_2 reduction occurs at the same rate by maintaining the ferrous ion concentration at a level much lower than that of the ferric ion. In the present work, rate equations are derived to explain the leaching results. As both pyrite oxidation [4, 5] and pyrolusite reduction [4, 6] are electrochemical in nature, polarization studies have been coupled with conventional leaching experiments to provide understanding of the process.

2. Theoretical background

Both MnO_2 and FeS_2 are semiconductors. When either is immersed in an electrolyte it develops a steady state (corrosion) potential similar to a corroding metal conductor. The following forward reactions are possible [4, 6]:

$$MnO_2 + 4\,H^+ + 2\,e^- = Mn^{2+} + 2\,H_2O \quad (4)$$

$$FeS_2 + 8\,H_2O = Fe^{2+} + 2\,SO_4^{2-} + 16\,H^+ + 14\,e^- \quad (5)$$

$$FeS_2 = Fe^{2+} + 2\,S^0 + 2\,e^- \quad (6)$$

In the presence of Fe^{3+}, Fe^{2+} the following reactions may result:

$$Fe^{3+} + e^- = Fe^{2+} \quad (7)$$

$$Fe^{2+} = Fe^{3+} + e^- \quad (8)$$

Thus, two corrosion couples occur when MnO_2 is dissolved in H_2SO_4 in the presence of FeS_2. Reactions 4 and 8 combine to form one couple and either or both of the reactions 5 and 6 combine with that represented by Equation 7 to form the other couple. Reaction 1 is the resultant of the former couple while Reactions 2 and 3 are the resultant of the latter. The reaction kinetics of such complex systems can be conveniently dealt with by plotting the current–potential curves for the respective half cells. These individual polarization curves, independently or with superimposition, provide useful information on the kinetics and mechanism of the process. Figure 1 depicts hypothetical polarization curves (Evans diagrams) for the present system. E_{MnO_2}, E_{FeS_2} and $E_{Fe^{3+}/Fe^{2+}}$ are the rest (steady state) potentials for the half cell reactions 4, 5 and 7/8, respectively. Reactions 3 and 6 are ignored for the sake of simplicity. The polarization plots (a)–(d) represent Reactions 4, 5, 7 and 8, respectively. In the absence of passivation, each of these plots normally show three stages, I, II and III, representing equilibrium, Tafel and limiting current regions, respectively. Superimposition of curves (b) and (c) indicate a mixed potential, E_m, and a mixed current, i_m for the second couple and superimposition of plots (a) and (d) indicate E'_m and i'_m as the respective parameters for the first couple. It also indicates that E'_m lies on (aI)–(dII) stages of the plots for the first couple and E_m lies on (bI) and (cII) of the plots for the second couple. Superimposition of plots (a) and (b) can also be used to obtain the galvanic potential (E_g) and current (i_g) for the galvanic interaction of the two minerals. This information is important in deriving the kinetic expressions for the particular process.

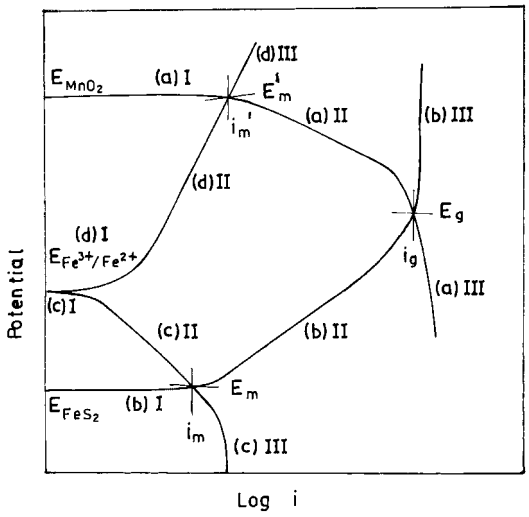

Fig. 1. Hypothetical Evans diagram for MnO_2 dissolution in H_2SO_4 in the presence of FeS_2.

Partial, as well as general, kinetic expressions can be derived for the particular corrosion coupling [7, 8]. In the present case the rate expression is first derived for the second couple from Reactions 5 and 7. It is also reported [4] that the mixed potential lies very close to the rest potential, E_{FeS_2}, on stage I of plot (b) and on stage II (Tafel region) of plot (c). Generally, the Butler–Volmer equation quantitatively describes such simple reversible reactions controlled by charge transfer [8]. The equations for stage I of plot (b) and stage II of plot (c) are as follows:

$$i_a = Z_a A_a F k_{af} \exp\left[\frac{\beta_a n_a FE}{RT}\right] - Z_a A_a F k_{ab}[Fe^{2+}][SO_4^{2-}][H^+] \times \exp\left[\frac{-(1-\beta_a) n_a FE}{RT}\right] \quad (9)$$

$$-i_c = Z_c A_c F k_{cf}[Fe^{3+}] \exp\left[\frac{-(1-\beta_c) n_c FE}{RT}\right] \quad (10)$$

For the purpose of simplification it can be assumed that $\beta_a = \beta_c = 1/2$ because experimental data on β for many corrosion reactions are in the range 0.4–0.6 [8]. Further, the value of n_a, n_c may also be assumed as unity since the rate controlling steps involve single electron transfer in such hydrometallurgical processes.

At E_m the partial currents i_a and $-i_c$ are equal and hence represented by Equation 11:

$$14A_a k_{af} \exp\left[\frac{FE_m}{2RT}\right] - 14A_a k_{ab}[Fe^{2+}][SO_4^{2-}][H^+] \times \exp\left[\frac{-FE_m}{2RT}\right] = 1A_c k_{cf}[Fe^{3+}] \exp\left[\frac{-FE_m}{2RT}\right] \quad (11)$$

Rearranging the terms gives the following expression for the mixed potential:

$$\exp\left[\frac{FE_m}{RT}\right] = \left(14A_a k_{ab}[Fe^{2+}][SO_4^{2-}][H^+] + A_c k_{cf}[Fe^{3+}]\right)/15A_a k_{af} \quad (12)$$

The rate of FeS_2 dissolution in this case is controlled by the cathodic reduction of Fe^{3+} ions since E_m is closer to E_{FeS_2} and further from $E_{Fe^{3+}}$. Thus, the rate of FeS_2 dissolution is equal to $-i_c$. Combining Equations 10 and 12 gives the following expression for FeS_2 dissolution:

$$\text{Rate} = \left(K_1[Fe^{3+}]/\{K_2[Fe^{3+}] + K_3[Fe^{2+}][SO_4^{2-}][H^+]\}^{1/2}\right) \quad (13)$$

As MnO_2 dissolution occurs at an equal rate to FeS_2 oxidation [4], Equation 13 should describe the dissolution rate. Since it is known that Reactions 3 and 6 also occur simultaneously [4, 9] another couple

consisting of Reactions 6 and 7, must also be considered. In this case the derived rate expression is similar to Equation 13 with different constant terms, but without the $[SO_4^{2-}]$ and $[H^+]$ terms. If MnO_2 reduction by ferrous ion, that is, the couple consisting of Equations 4 and 8 occurs at slower speed, the rate expression for MnO_2 dissolution is different. Considering the combination of (aI)–(dII) [4] and $i'_a = -i'_c$ at E'_m the following relation ensues:

$$1A'_aFk'_{af}[Fe^{2+}]\exp\left(\frac{FE'_m}{2RT}\right) = 2A'_cFk'_{cf}[H^+]\exp\left(\frac{-FE'_m}{2RT}\right) - 2A'_cFk_{cb} \times [Mn^{2+}]\exp\left(\frac{FE'_m}{2RT}\right) \quad (14)$$

or

$$\exp\left(\frac{FE'_m}{RT}\right) = (2A'_ck'_{cf}[H^+])/(A'_ak'_{af}[Fe^{2+}] + 2A'_ck_{cb}[Mn^{2+}]) \quad (15)$$

Since E'_m is closer to E_{MnO_2} and further from $E_{Fe^{2+}}$, the oxidation of ferrous ion, that is, i'_a controls the reaction. Using the expression for i'_a along with Equation 15, the following rate expression results:

$$\text{Rate} = \frac{\left(K_4[Fe^{2+}]\{[H^+]\}^{1/2}\right)}{\left(K_5[Fe^{2+}] + K_6[Mn^{2+}]\right)^{1/2}} \quad (16)$$

Another situation may arise for the corrosion couple depicted in Fig. 2 for the FeS_2/Fe^{3+} system represented by Equations 5 and 7. The Figure represents two specific cases denoted by (E_{m1}, i_{m1}) and (E_{m2}, i_{m2}). The two cases presented in Fig. 2 are feasible but depend on the Fe^{3+} and Fe^{2+} concentrations. Increase in the Fe^{3+} concentration shifts the system towards case 2 while increase in the Fe^{2+} concentration shifts the system towards case 1. The derivation presented in the previous paragraphs corresponds to the second case. In the event of the leaching as per case 1, this particular derivation for i_m (Equation 13) does not hold good because, $i_{FeS_2(corr)}$, which may be termed as the self corrosion of the FeS_2 electrode, controls the process. $i_{FeS_2(corr)}$ may then be derived from Equation 9 as follows:

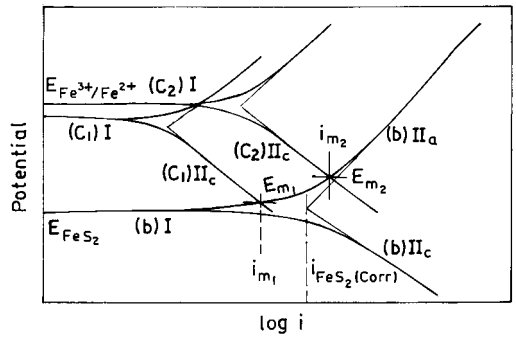

Fig. 2. Hypothetical Evans diagram for FeS_2 dissolution at specific conditions.

$$i_{FeS_2(corr)} = 15A_ak_{af}\exp\left(\frac{FE}{2RT}\right) = 15A_ak_{ab}[Fe^{2+}][SO_4^{2-}][H^+] \quad (17)$$

A careful examination of Equations 13 and 17 reveals that increase in $[Fe^{3+}]$ and decrease in $[Fe^{2+}]$ and $[H^+]$ pushes the process towards higher i_m, that is, towards the case 2 of Fig. 2 and hence Equation 13 should hold good. Conversely, decrease of $[Fe^{3+}]$ and increase in $[Fe^{2+}]$ and $[H^+]$, results in a decrease in i_m and increase in $i_{FeS_2(corr)}$ so that Equation 17 applies. This analysis also applies for MnO_2/Fe^{2+} couple.

The present study examines some of these aspects using experimental data for MnO_2 dissolution in the presence of pyrite in H_2SO_4 medium.

3. Experimental details

Synthetically prepared β-MnO_2 containing 62.11% Mn^{4+} and high grade crystalline pyrite (Amjhor pyrite deposit of Bihar, India) with 42.76% Fe and 47.88% S were used for the polarization studies. Electrodes were prepared by pressing for 30 min in a cylindrical stainless steel mould of 2.5 cm diameter under 0.34 kbar at 130 ± 5 °C. Each electrode contained 5 g of either β-MnO_2 or pyrite along with 1 g of graphite to increase the conductivity and 0.6 g of transoptic powder (Buehler Ltd, USA) as binder. One conducting wire was attached to one plane face of the compressed pellet using a silver based conducting cement and was then mounted using Araldite to establish an ohmic contact. The geometric surface area of the open face was 5 cm^2.

Polarization curves were plotted using a three electrode cell. Platinum was used as the counter electrode for MnO_2 or FeS_2. For the redox couple of Fe^{3+}/Fe^{2+}, platinum was used as the working electrode and MnO_2/FeS_2 as the counter electrode. A saturated calomel electrode served as the reference electrode. A model 362 scanning potentiostat (EG & G PARC) coupled with series 2000 Omnigraphic recorder was used to plot the polarization curves.

For particulate leaching experiments, a low grade manganese ore from the Nishikhal deposits of Orissa, India, of size −90 + 70 μm, containing 58.41% MnO_2 with goethite and silicates as gangue and a shaly pyrite, of 85% −90 μm size, containing 25% FeS_2 with silica and alumina as major gangue were used. The leaching experiments were conducted in a stirred two litre flanged glass reactor with lid which was heated in a thermostatic bath to maintain the temperature within ±1 °C. Chemicals used were of reagent grade. More details about the experimental procedures were described earlier [4–6].

4. Results

Figure 3 shows Evans diagram for the MnO_2–FeS_2 system at 30 °C in 0.1 M H_2SO_4. Plots (a) and (b)

represent potentiostatic polarization, whereas plots (c) and (d) represent galvanostatic polarization for FeS_2 and MnO_2 electrodes, respectively. Plots (e) are drawn for platinum electrode in 0.0002 M Fe^{2+}, 0.003 M Fe^{3+} and 0.1 M H_2SO_4 solution. In this case the cathodic plot represents Reaction 7 and the anodic plot Reaction 8. The intersection point X between the superimposed anodic (c) and cathodic (e) plots corresponds to the second couple FeS_2/Fe^{3+} (Fig. 1). Similarly, the intersection point Y between anodic (e) and cathodic (d) represents the first couple, MnO_2/Fe^{2+} (Fig. 1). The experimentally observed parameters are $E_m = 0.400$ V, $i_m = 0.16$ mA cm^{-2}, $E'_m = 0.845$ V and $i'_m = 0.15$ mA cm^{-2}. The five star marked points 1 to 5 shown in Fig. 3 represent experimentally observed dissolution rates converted to current equivalents at 30 °C in 0.1 M H_2SO_4 as follows:

Star 1: For FeS_2 electrode (i_{corr} for FeS_2)
Star 2: For MnO_2 electrode (i_{corr} for MnO_2)
Star 3: For MnO_2 electrode when externally connected to FeS_2 (i_g for MnO_2 in MnO_2–FeS_2 couple)
Star 4: For FeS_2 electrode when externally connected to MnO_2 (i_g for FeS_2 in MnO_2–FeS_2 couple)
Star 5: For MnO_2 dissolution in particulate leaching in presence of FeS_2. Density and size of particles were used to calculate surface area.

The closeness of the electrochemically observed reaction rates with those determined from leaching studies suggest that leaching of MnO_2 in acid medium in presence of pyrite proceeds as indicated under theoretical section.

Figure 4 presents the leaching results of 10 g MnO_2 ore with 19.2 g FeS_2 ore in 1.5 dm^3 0.1 M H_2SO_4 at 100 °C. Mn^{2+} steadily builds up along with Fe_T with time. There is little difference between $[Fe_T]$ and $[Fe^{3+}]$ up to about 60 min. Then $[Fe^{2+}]$ builds up at the cost of $[Fe^{3+}]$. $[SO_4^{2-}]$ shows a steep rise initially and then continues to rise at a slower rate. $[H^+]$ follows an identical pattern with a high rate of loss in the first few minutes and then a steady rate. After 60 min the rate is almost constant. This may be due to depletion of MnO_2 by this time and only the second couple remains active. Therefore, results upto 60 min are considered for interpretation.

A combination of Reactions 1 and 2 gives the stoichiometry in the absence of Reaction 3. Since the major iron product during the first 60 min is Fe^{3+} ion, the final reaction is

$$FeS_2 + 7.5\ MnO_2 + 14\ H^+ = 7.5\ Mn^{2+} + Fe^{3+} + 7\ H_2O + 2\ SO_4^{2-} \quad (18)$$

Table 1 presents some important parameters related to reaction stoichiometry. Fe_T production is slightly higher than indicated by Equation 18, which may be due to dissolution also through Equation 3. Analysis of the final residue indicates that about one fourth of the dissolved pyrite produces S^0. Combining this proportion of Reaction 3 with Reaction 18 results in a Fe_T/Mn^{2+} ratio of 0.267. As the accuracy of S^0 determination is only moderate, the experimental result can be considered to satisfy the stoichiometry of Equation 18. Reaction 3 is ignored for the kinetic equation because its contribution in terms of electrons is hardly 5% even if 25% of FeS_2 forms S^0.

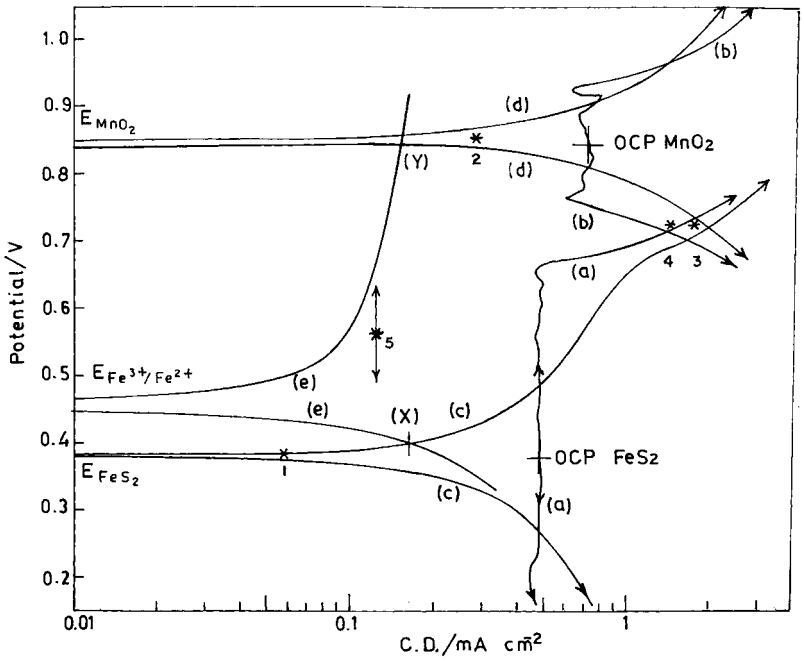

Fig. 3. Evans diagram for MnO_2–FeS_2 system at 30 °C. Potentiostatic plots for (a) FeS_2 (1 mV s^{-1}) and (b) MnO_2 (0.5 mV s^{-1}) in 0.1 M H_2SO_4. Galvanostatic plots for (c) FeS_2 (0.1 mA s^{-1}) and (d) MnO_2 (0.1 mA s^{-1}) in 0.1 M H_2SO_4. Galvanostatic plots for (e) Pt (0.1 mA s^{-1}) in (0.0002 M Fe^{2+} + 0.003 M Fe^{3+} + 0.1 M H_2SO_4). Star marked points indicate experimental leaching rates converted to current equivalents: open circuit dissolution of (1) FeS_2, (2) MnO_2; galvanic dissolution of (3) MnO_2, (4) FeS_2 all in 0.1 M H_2SO_4 and (5). Particulate MnO_2–FeS_2 dissolution rate in 0.1 M H_2SO_4.

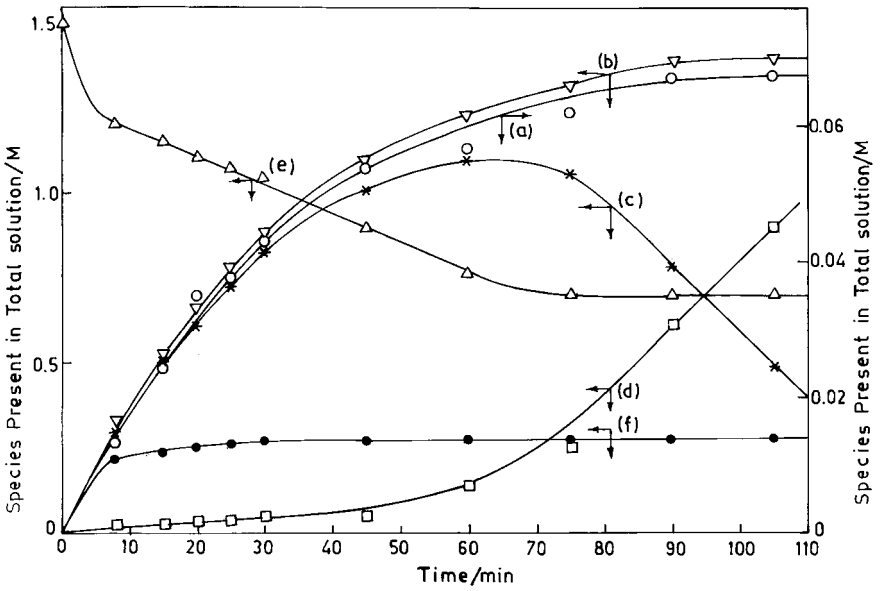

Fig. 4. Dissolution of MnO_2–FeS_2 in 0.1 M H_2SO_4 at 100 °C. MnO_2 ore: 10 g; FeS_2 ore: 19.2 g, H_2SO_4: 1.5 dm^3. (a) $[Mn^{2+}]$, (b) $[Fe_T]$ (scale $\times 10^{-2}$), (c) $[Fe^{3+}]$ ($\times 10^{-2}$), (d) $[Fe^{2+}]$ ($\times 10^{-2}$), (e) $[H_2SO_4]$ ($\times 10^{-1}$) and (f) $[SO_4^{2-}]$.

Table 1. Reaction stoichiometry with respect to different species obtained from Fig. 4

Time/min	8	15	20	25	30	45	60	*Eqn 18*
$(*Fe_T/Mn^{2+})$	0.244	0.217	0.192	0.206	0.204	0.201	0.217	0.133
$(-)(H^+/Mn^{2+})$	2.667	1.901	1.518	1.493	1.392	1.484	1.767	1.867

$*Fe_T \sim Fe^{3+}$.

Equations 13, 16 and 17 were tested for these data to determine their validity. Usually this is done by fixing the concentrations of all but one of the species in the experiments. Then the equation is tested for the experimental data for varying concentrations of the remaining species. Figure 4, however, suggests that maintaining a constant concentration of either of the species involved in such experiments is difficult. Therefore, a different approach [10] was adopted to check the collective effect of all the species on the dissolution rate by using parameters obtained from Fig. 4 at different times. The manganese dissolution rate was obtained as slopes at these times and the corresponding concentrations of Fe^{3+} and other species were known. Thus, Equations 13 and 16 are verified in Fig. 5. For this purpose, these two equations are reorganized as follows:
for Equation 13

$$[Fe^{3+}]/(\text{Rate})^2 = K_7([Fe^{2+}][H^+][SO_4^{2}]/[Fe^{3+}]) + K_8 \quad (19)$$

for Equation 16

$$([Fe^{2+}]\,[H^+])/(\text{Rate})^2 = K_9\,([Mn^{2+}]/[Fe^{2+}]) + K_{10} \quad (20)$$

Figure 5(a) relates to Equation 19 and Fig. 5(b) to Equation 20; these reveal interesting trends. The data for the initial 25 min satisfy Equation 20, whereas those from 25 to 60 min satisfy Equation 19. This implies that dissolution of the first couple, MnO_2/Fe^{2+}, is slower initially, while dissolution of the second couple, FeS_2/Fe^{3+}, is slower at later stages of the reaction. This is possible because slight increase in $[Fe^{2+}]$ increases the MnO_2 dissolution to a relatively greater extent than that in $[Fe^{3+}]$ to FeS_2 dissolution, as demonstrated in Fig. 6. Plots (c) and (d) are, respectively, for $[Fe^{2+}]$, $[Fe^{3+}]$ prevailing in the conditions of Fig. 4 at initial and final stages of leaching. The current at the intersection point of anodic (c) and cathodic (b) plots is less than that at the intersection point of the anodic (a) and cathodic (c) plots at the electrolyte conditions prevalent during the initial periods. This is reversed during the later periods as the electrolyte conditions change.

The next experiment was conducted in 0.25 M H_2SO_4 keeping other conditions identical. In the first 45 min only MnO_2 was allowed to dissolve and there was very little dissolution. The dissolution increased on adding pyrite ore. Figure 7 presents the leaching results. It is interesting to note that $[Fe^{2+}]$ and $[Fe^{3+}]$ do not differ much during the initial stages when compared with the results of 0.1 M H_2SO_4 (Fig. 4). However, $[Fe^{2+}]$ concentration remained static for about 20 min in the present case and so also the dissolution rates of MnO_2 and FeS_2. Afterwards, the rates of MnO_2 and FeS_2 dissolution decreased continuously with increase in time and $[Fe^{2+}]$. The parameters related to reaction stoichiometry are presented in Table 2.

Kinetic Equations 17, 19 and 20 were tested for these data in a similar way. The constant rate of

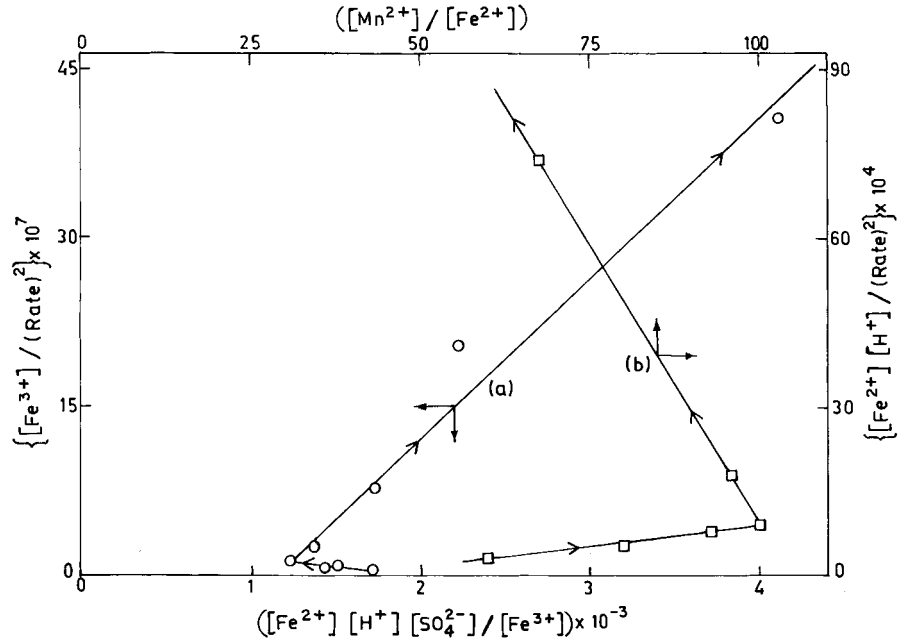

Fig. 5. Kinetic relation for MnO_2–FeS_2 dissolution in 0.1 M H_2SO_4 at 100 °C. (a) $[Fe^{3+}]/(rate)^2$ against $([Fe^{2+}]\,[H^+]\,[SO_4^{2-}]/\,[Fe^{3+}])$ and (b) $([Fe^{2+}]\,[H^+])/(rate)^2$ against $[Mn^{2+}]/[Fe^{2+}]$ plots. Arrow indicates direction of progress (time).

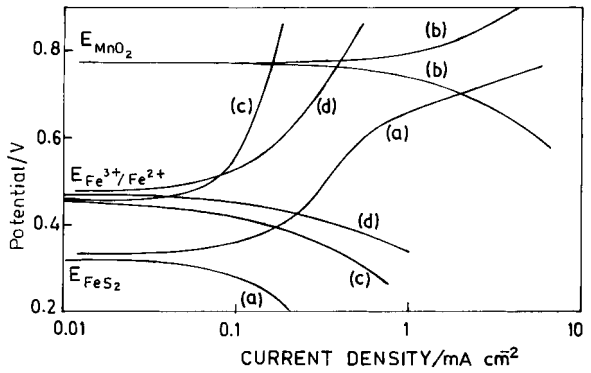

Fig. 6. Galvanostatic (0.1 mA s^{-1}) polarization plots for MnO_2–FeS_2 system at 30 °C. (a) for FeS_2 in 0.07 M H_2SO_4, (b) for MnO_2 in 0.07 M H_2SO_4, (c) for Pt in (0.07 M H_2SO_4 + 0.0002 M $FeSO_4$ + 0.003 M $Fe_2(SO_4)_3$) and (d) for Pt in (0.07 M H_2SO_4 + 0.005 M $FeSO_4$ + 0.01 M $Fe_2(SO_4)_3$).

dissolution and constant $[Fe^{2+}]$ level may indicate the dissolution due to first couple, MnO_2/Fe^{2+}, as slower and rate controlling. However, the corresponding equation (Equation 20) does not satisfy the data. On the otherhand rate control by the second couple, FeS_2/Fe^{3+}, occurring at a constant rate even with increase in $[Fe^{3+}]$, is possible only when Equation 17 holds good. Figure 8 verifies this aspect where the first seven points in plot (a), that is, up to 30 min of dissolution merge at a close region suggesting validity of case 1 of Fig. 2. Later, the rate decreases even though $([Fe^{2+}]\,[H^+][SO_4^{2-}])$ increases. Plot (b) representing Equation 19 shows a straight line after 30 min suggesting that case 2 of Fig. 2 operates beyond 30 min. This change may be due to rise in $[Fe^{3+}]$. Beyond 50 min of dissolution only the second couple is active.

The effect of increased $[Fe^{3+}]$ and $[Fe^{2+}]$ through an increase in percentage solids as well as $[H^+]$ was studied by charging an ore containing 25% Mn. This charge may also indicate the effect of ore body, if any. Figure 9 presents the leaching data on 100 g of MnO_2 and 120 g of FeS_2 with 1 dm^3 of 1.5 M H_2SO_4 at 100 °C. The results were identical to that of Fig. 7, that is, a constant $[Fe^{2+}]$, constant dissolution rates for MnO_2 and FeS_2 with increased $[Fe^{3+}]$ prevailing initially. $[Fe^{3+}]$ and $[Fe^{2+}]$ were much higher in comparison to those of Fig. 7. Table 3 presents the parameters related to reaction stoichiometry which are also identical to those presented in Table 2.

Kinetic Equations 17, 19 and 20 were tested for these data also. Equation 20 does not hold good and the other equations were verified in Fig. 10. Here also the process is controlled by self corrosion of FeS_2 initially and by the mixed potential presented in case 2 of Fig. 2 subsequently. Only pyrite dissolves after all the MnO_2 is consumed. The entire process is quicker at higher acid concentration.

These experiments already indicate that both the couples occur as depicted in the theoretical section. At lower acid conditions dissolution due to MnO_2/Fe^{2+} proceeds at a slower rate than the dissolution due to the other couple, FeS_2/Fe^{3+}, during the initial period of leaching. Subsequently the first couple becomes faster due to Fe^{2+} build-up and the second couple becomes slower and controls the overall process. Higher acid concentration helps the latter situation. However, occurrence of case 1 or case 2 of Fig. 2 is decided by the $[Fe^{3+}]$; higher $[Fe^{3+}]$ favours case 2.

5. Discussion

The point of focus in this complicated process is the occurrence of two corrosion couples MnO_2/Fe^{2+} and FeS_2/Fe^{3+} which maintain a balance between them. Neither MnO_2 nor FeS_2 react favourably in H_2SO_4

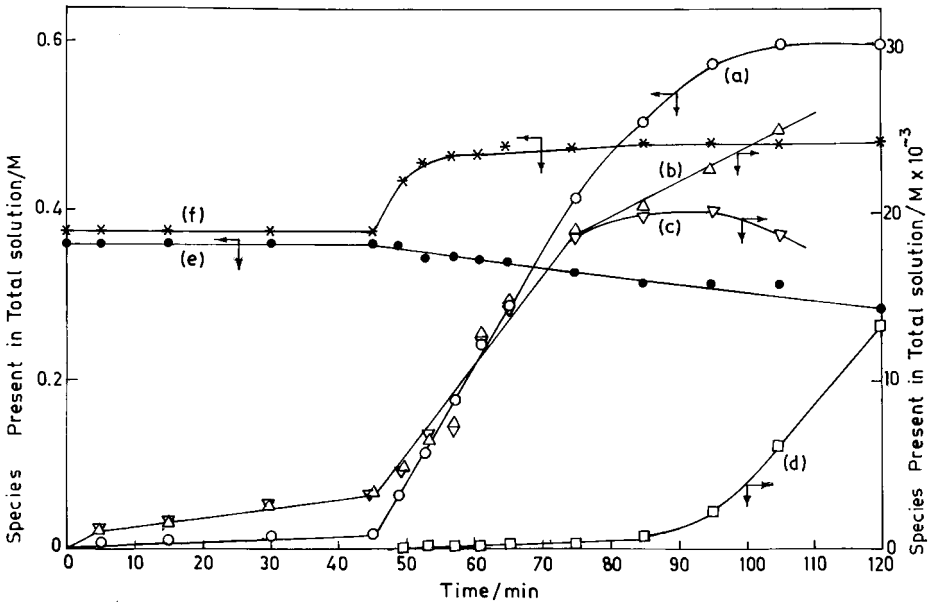

Fig. 7. Dissolution of MnO_2–FeS_2 in 0.25 M H_2SO_4 at 100 °C. MnO_2 ore: 10 g; FeS_2 ore: 19.2 g; H_2SO_4: 1.5 dm^3. (a) $[Mn^{2+}]$ (scale $\times 10^{-1}$), (b) $[Fe_T]$, (c) $[Fe^{3+}]$, (d) $[Fe^{2+}]$, (e) $[H_2SO_4]$ and (f) $[SO_4^{2-}]$.

Table 2. Reaction stoichiometry with respect to different species obtained from Fig. 7

Time/min (*Reaction time*)	49 (4)	53 (8)	57 (12)	61 (16)	65 (20)	75 (30)	85 (40)	*Eqn 18*
(Fe_T^*/Mn^{2+})	0.369	0.369	0.250	0.427	0.403	0.391	0.346	0.133
$(-)(H^+/Mn^{2+})$	2.289	3.169	1.862	1.324	1.099	1.505	1.841	1.867

*$Fe_T \sim Fe^{3+}$.

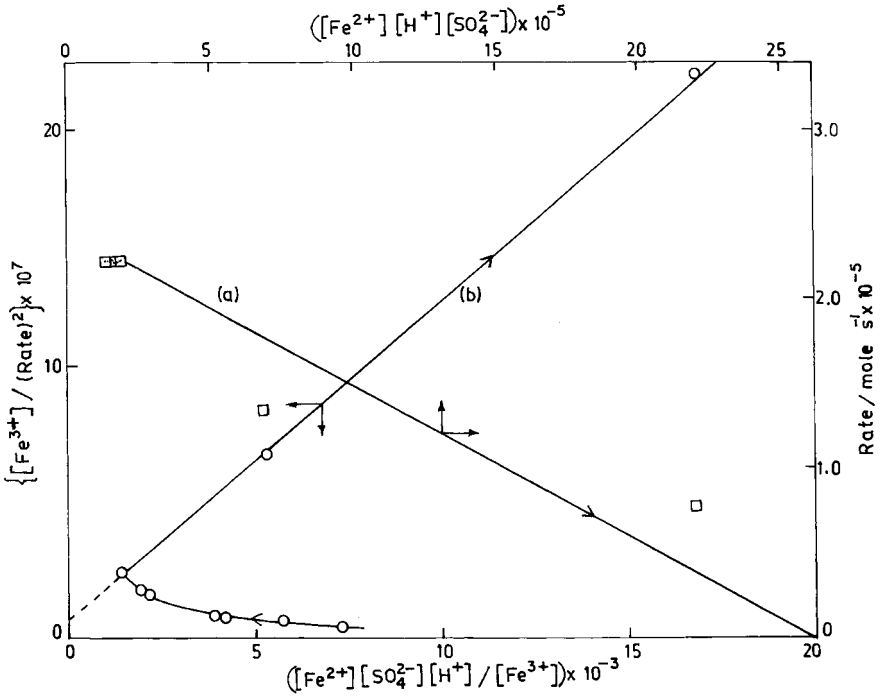

Fig. 8. Kinetic relation for MnO_2–FeS_2 dissolution in 0.25 M H_2SO_4 at 100 °C. (a) rate against $([Fe^{2+}]\,[H^+]\,[SO_4^{2-}])$ and (b) $([Fe^{3+}]/(\text{rate})^2)$ against $([Fe^{2+}]\,[H^+]\,[SO_4^{2-}]/\,[Fe^{3+}])$ plots. Arrow indicates direction of progress (time).

solution but dissolve very quickly only if they are immersed together. This may be due to the cyclic action of the Fe^{3+}/Fe^{2+} couple as depicted in the theoretical section. The other possibility of the galvanic interaction between MnO_2–FeS_2 has not been discussed because, in an earlier study [4], negligible galvanic interaction between these two minerals was reported at identical solid–liquid ratio. This has been

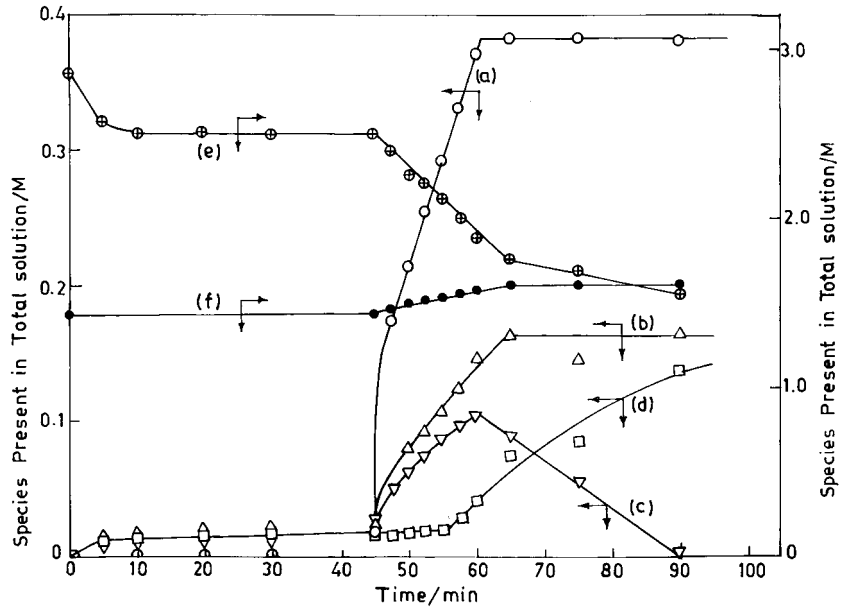

Fig. 9. Dissolution of MnO_2–FeS_2 in 1.5 M H_2SO_4 at 100 °C. MnO_2 ore: 100 g (25% Mn); FeS_2 ore: 120 g (13.35% S); H_2SO_4: 1 dm^3. (a) $[Mn^{2+}]$, (b) $[Fe_T]$, (c) $[Fe^{3+}]$, (d) $[Fe^{2+}]$, (e) $[H^+]$ and (f) $[SO_4^{2-}]$.

Table 3. Reaction stoichiometry with respect to different species obtained from Fig. 9

Time/min (*Reaction time*)	47.5 (2.5)	50 (5)	52.5 (7.5)	55 (10)	57.5 (12.5)	60 (15)	*Eqn 18*
(Fe_T/Mn^{2+})	0.393	0.368	0.366	0.365	0.374	0.401	0.133
$(-)(H^+/Mn^{2+})$	0.571	1.203	1.139	1.263	1.449	1.690	1.867

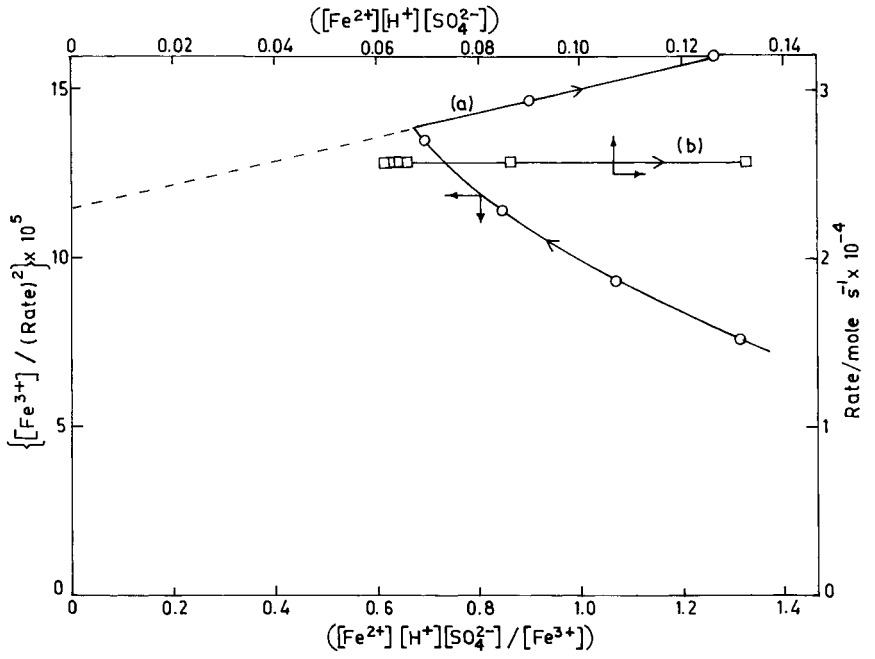

Fig. 10. Kinetic relation for MnO_2–FeS_2 dissolution presented in Fig. 9. (a) $([Fe^{3+}]/(rate)^2)$ against $([Fe^{2+}]\,[H^+]\,[SO_4^{2-}]/\,[Fe^{3+}])$, (b) rate against $([Fe^{2+}]\,[H^+]\,[SO_4^{2-}])$. Arrow indicates direction of progress (time).

ascribed to poor contact in a dilute slurry. It is presumed that galvanic interaction would have resulted in a higher dissolution rate represented by stars 3 or 4 in Fig. 3, rather than the lower one of star 5. It may be argued that a rate represented by star 5 is also practically feasible due to galvanic interaction with partial contact rather than due to cyclic action of Fe^{3+}/Fe^{2+} couple. Recently, galvanic interaction between these two minerals has been studied in detail [11, 12]. These reports as well as Fig. 3 of this study

suggest that the interaction takes place in the Tafel regions of both the anodic and cathodic half processes. A combination of (aII)–(bII) (Fig. 3) results in the following expression for i_g:

$$i_g = K_{11}\,[H^+]^{1/2} \qquad (21)$$

This implies that the dissolution rate by galvanic interaction depends only on $[H^+]^{1/2}$. However, in Figs 7 and 9 the dissolution rate remains constant during certain periods even though $[H^+]$ keeps on decreasing. Therefore, the possibility of a major role for galvanic interaction is ruled out in this process.

In the cyclic action of Fe^{3+}/Fe^{2+}, balancing of the corrosion couples in terms of total mixed current in each case is a critical factor. Understanding of this aspect is important to clarify the reaction mechanism. In the present investigation, the rates of MnO_2 and FeS_2 dissolution $\left(\text{mole s}^{-1}\right)$ maintain a constant ratio. It is about 5 for the first experiment and about 2.5 in the next two. This number appears to be linked to the stoichiometry of the reactions. When FeS_2 dissolution follows Equation 5 only, this ratio is 7.5 and is 1.33 if Equation 6 only is followed. Naturally, a ratio of 5 or 2.5 implies simultaneous occurrence of Reactions 5 and 6. Also the ratio of $i_{MnO_2(corr)}$ and, $i_{FeS_2(corr)}$, (stars 2 and 1 in Fig. 3) is nearly 5. Whether the reaction stoichiometry is involved in this case is not known but this number assumes significance. The balancing mechanism of these two corrosion couples may be better understood by extending the aspects presented in the theoretical section. As both these couples, FeS_2/Fe^{3+} and MnO_2/Fe^{2+}, occur at mixed potentials close to the rest potentials of FeS_2 and MnO_2, respectively, cases 1 and 2 of Fig. 2 are applicable to either of them. The following four situations arise.

Situation A: This arises when both FeS_2/Fe^{3+} and MnO_2/Fe^{2+} couples follow case 1. Figure 11 shows the polarization curves for these two couples along with their self corrosion current when $[H^+]$ in the electrolyte varies. In either case $i_{(corr)}$ increases with $[H^+]$ and $i_{MnO_2(corr)}$ is greater than $i_{FeS_2(corr)}$ at constant $[H^+]$. The effect of $[Fe^{2+}]$ or $[Fe^{3+}]$ have not been tested as these species result in mixed potentials. However, Fe^{3+}/Fe^{2+} effect, at concentrations corresponding to the initial and final stages of leaching experiments, is superimposed in Fig. 11. Theoretically, $i_{FeS_2(corr)}$ depends on $[Fe^{2+}][SO_4^{2-}]$ $[H^+]$ and $i_{MnO_2(corr)}$ on $[H^+]$ or $[Mn^{2+}]$. Thus H^+ becomes the balancing species. Based on the observations from Fig. 11 the possibility of this situation occurring is remote, though the initial portion of the second experiment may come under this category.

Situation B: This arises when both the couples follow case 2 and is dealt in detail in the theoretical section with Equations 13 and 16 representing the rate expressions of these two couples. H^+, Fe^{3+} and Fe^{2+} species play the balancing role. Obviously, Fe^{3+} and Fe^{2+} together, but not individually, are involved in Equation 13 in a way that when one changes the other also changes. The first experiment (Fig. 4) and the latter portion of Experiment 3 are of this category.

Situation C: This arises when FeS_2/Fe^{3+} follows case 2 but MnO_2/Fe^{2+} follows case 1. Here Equation 13 describes FeS_2 dissolution while $[H^+]$ or $[Mn^{2+}]$ controls $i_{MnO_2(corr)}$. Therefore, $[H^+]$ is again the bal-

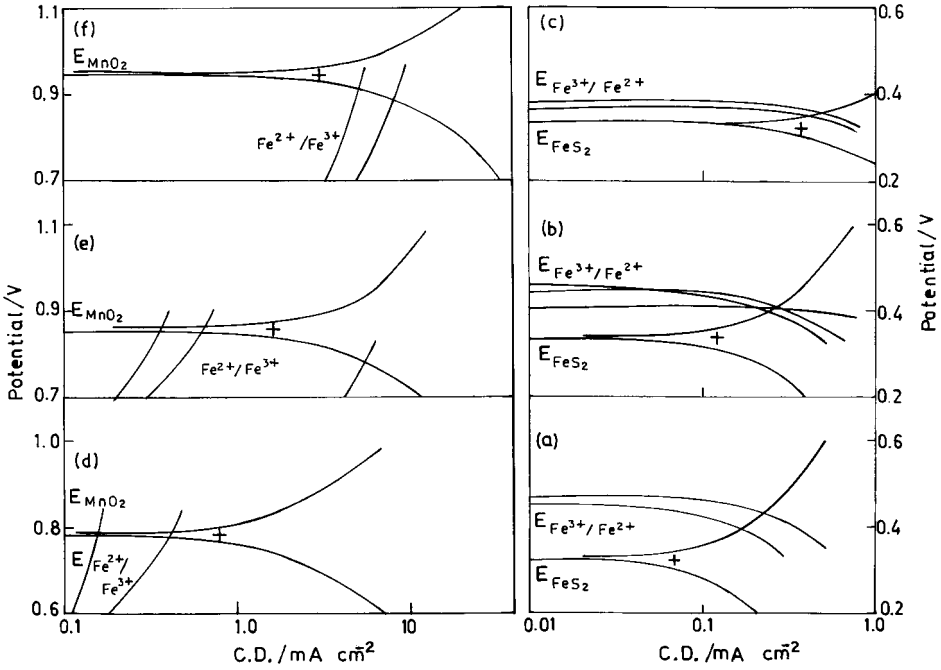

Fig. 11. Galvanostatic polarization plots (1 mA s^{-1}) for FeS_2–MnO_2 system at 30 °C. (a) and (d) at 0.07 M H_2SO_4, (b) and (e) at 0.25 M H_2SO_4, (c) and (f) at 1.2 M H_2SO_4.

ancing factor. The latter portion of the second experiment belongs to this category.

Situation D: This arises when FeS_2/Fe^{3+} follows case 1 but MnO_2/Fe^{2+} follows case 2. The initial portion of experiment 3 probably belongs to this category. Since i_m for MnO_2/Fe^{2+} is always larger than either $i_{FeS_2(corr)}$ or i_m of the FeS_2/Fe^{3+} couple, specifically at higher acid concentrations, the rate control is almost identical to that of situation A with the difference that, in this case both $[H^+]$ and $[Fe^{2+}]$ play the balancing role.

Evidently, the experiments presented in this study resulted in very good MnO_2 dissolution, even up to completion, in all the cases. The above analysis indicates that leaching is effective even when more than stoichiometric quantities of acid (for Equation 4) is available at a reasonable concentration to avoid iron precipitation (> 0.1 M). The presence of Fe^{3+} assists the process.

MnO_2 also dissolves well in low acid conditions. However, further studies are required to establish the process details in such conditions.

6. Conclusions

The following conclusions may be drawn from the present study:

(a) Polarization studies help to understand the complicated process of MnO_2 dissolution in H_2SO_4 in the presence of FeS_2.
(b) The dissolution occurs mostly through two corrosion couples of FeS_2/Fe^{3+} and MnO_2/Fe^{2+} balancing the total corrosion current (dissolution rate) in each case.
(c) The reactant and product species play balancing roles in the process by adjusting their concentrations.
(d) When sufficient acid is present, dissolution due to FeS_2/Fe^{3+} proceeds at a slower rate thus controlling the process.
(e) As the couple, FeS_2/Fe^{3+}, mostly occurs at a potential close to the rest potential of FeS_2, its self corrosion, $i_{FeS_2(corr)}$, also plays an important role in the rate limiting process.
(f) Application of corrosion principles through the Butler–Volmer equation leads to derive kinetic expressions for the system. These equations can be validated with experimental data obtained from leaching studies.

Acknowledgements

The authors thank Prof. H. S. Ray, Director, RRL, Bhubaneswar for his keen interest in this work and giving permission for publication of this paper. Thanks are also due to Nishikhal mines, Orissa, Amjhor Pyrite deposits, Bihar and Tata Steel, Jamshedpur for providing samples. The authors also wish to thank Dr J. R. Rao, Scientist, RRL- Bhubaneswar for his help in preparation of this manuscript.

References

[1] B. J. P. Whalley, D. E. Pickett, R. F. Pilgrim and T. R. Ingraham, *Indian Mining. J.* (1957) 61.
[2] G. Thomas and B. J. P. Whalley, *Can. J. Chem. Engng.* **36** (1958) 37.
[3] R. J. Cornelius and J. T. Woodcock, *Aus IMM Proc.* **185** (1958) 65.
[4] B. B. Nayak, K. M. Parida, S. B. Rao and R. K. Paramguru, *ibid.* **300** (1995) 79.
[5] B. B. Nayak, R. K. Paramguru and H. S. Ray, *Trans. Indian Inst. Met.* **48** (1995) 35.
[6] B. B. Nayak, R. K. Paramguru and H. S. Ray, *Trans. Indian Inst. Met.* **48** (1995) 29.
[7] R. K. Paramguru and H. S. Ray, *Min. Pro. Extr. Met. Rev.* **16** (1996) 63.
[8] M. E. Wadsworth, Heterogeneous Rate Processes in the leaching of base metal sulphides, in 'Hydrometl. Process Fundamentals' (edited by R. Bautista), *NATO Conf. Ser.* **6** (1984) 41.
[9] P. C. Rath, R. K. Paramguru and P. K. Jena, *Trans. Indian Inst. Met.* **42** (1989) 321.
[10] R. K. Paramguru and S. B. Kanungo, *Trans. Indian Inst. Met.* **48** (1995) 301.
[11] B. B. Nayak, K. M. Parida, S. B. Rao, R. K. Sahoo and R. K. Paramguru, *Trans. Indian Inst. Met.* **47** (1994) 27.
[12] R. K. Paramguru and B. B. Nayak, *J. Electrochem. Soc.* **143** (1996) 3987.